Fermi Surface of the Heavy-fermion Superconductor PrTi2Al20

Kubo, Tomoya ; Matsuoka, Eiich ; Kotegawa, Hisashi ; Tou, Hideki ; Nakamura, Ai ; Aoki, Dai ; Harima, Hisatomo ; Sugawara, Hitoshi

(Citation)
Journal of the Physical Society of Japan,89(8):084704

(Issue Date)
2020-08-15

(Resource Type)
journal article

(Version)
Accepted Manuscript

Fermi Surface of the Heavy-fermion Superconductor $PrTi_2Al_{20}$

Tomoya Kubo[1], Eiich Matsuoka[1], Hisashi Kotegawa[1], Hideki Tou[1], Ai Nakamura[2], Dai Aoki[2], Hisatomo Harima[1], and Hitoshi Sugawara[1*]

[1] *Graduate School of Science, Kobe University, Kobe, Hyogo 657-8501, Japan*

[2] *IMR, Tohoku University, Oarai, Ibaraki 311-1313, Japan*

(Accepted Jun 24, 2020)

We have investigated the Fermi surface properties in the Pr-based heavy-fermion superconductor $PrTi_2Al_{20}$ and its reference compound $LaTi_2Al_{20}$ by means of the de Haas-van Alphen effect experiments and the band-structure calculation. The topology of Fermi surface in $PrTi_2Al_{20}$ is close to that of the reference compound $LaTi_2Al_{20}$, indicating a localized nature of 4*f*-electrons. Whereas the localized nature of 4*f*-electrons, we have confirmed a highly enhanced cyclotron effective mass up to 12 m_0 (m_0 is a rest mass of electron), which is enhanced about 5 times compared to that in $LaTi_2Al_{20}$.

KEYWORDS: $PrTi_2Al_{20}$, heavy-fermion superconductor, quadrupole order, de Haas-van Alphen effect, band-structure calculation, Fermi surface

1. Introduction

Rare-earth intermetallic compounds RT_2Al_{20} (R = rare-earths, T = Ti, V, Cr) with cubic $CeCr_2Al_{20}$-type structure (space group No. 227, $Fd\bar{3}m$, O_h^7) have attracted much attention because of their fascinating unusual properties, such as a heavy-fermion superconductivity in the proximity of quadrupole (or multipole) order in PrT_2Al_{20} (T = V, Ti),[1-4] Nd-based heavy-fermion behavior in ferromagnetic NdV_2Al_{20},[5] and a field-insensitive heavy-fermion behavior in $SmTi_2Al_{20}$.[6, 7] Among them, $PrTi_2Al_{20}$ undergoes a superconducting transition at T_c = 0.2 K in the ferro-quadrupole ordered state below T_{FQ} = 2.0 K.[1, 2] The specific heat measurement under an ambient pressure revealed the Sommerfeld coefficient $\gamma \sim 100$ mJ/(K^{2}mol) and the moderately large effective mass $m^* \sim 16\ m_0$ (m_0 is a rest mass of electron) was suggested from the temperature dependence of the superconducting upper critical field.[2] The specific heat and magnetic susceptibility measurements revealed that the crystalline electric field (CEF) ground state of Pr^{3+} ions have the non-magnetic Γ_3 doublet,[2] and the inelastic neutron scattering experiment confirmed the CEF level scheme consisting of Γ_3 doublet ground state, Γ_4 triplet at 65 K, Γ_5 triplet at 108 K, and Γ_1 singlet at 156 K.[8] The ultrasonic experiment revealed that a coupling constant of inter-site interaction between the quadrupole moments is positive, suggesting a ferro-type quadrupolar interation,[9] and the neutron diffraction and the NMR experiments provided the evidence of ferro-quadrupole order below T_{FQ}.[8, 10] Since the exciting energies of the CEF states are much larger than the energy scales of quadrupolar interaction, active degrees of freedom of Γ_3 doublet should be responsible for the physical properties at low temperatures. The temperature dependence of electrical resistivity $\rho(T)$ shows a $-\ln T$ dependence at high temperatures with a peak at around 50 K, which might be due to a conventional Kondo effect originated from the excited magnetic triplets, while $\rho(T)$ shows T^2 dependence below $\sim$ 20 K indicating Fermi liquid behavior.[1, 2] Moderately strong *c*-*f* hybridization between the conduction(*c*)- and 4*f*-electrons was inferred from the Kondo resonant peak observed in the photoemission spectroscopy.[11] Under the high pressure, T_{FQ}

slightly increases with increasing pressure up to ~ 7 GPa above which it suddenly decreases with increasing pressure, and the superconducting transition temperature and the effective mass are dramatically enhanced as the system approaches to the quantum critical point (QCP) of the ferro-quadrupole order, i.e., T_c = 1.1 K and m^* ~ 106 m_0 at the pressure P = 8.7 GPa.[3] These facts suggest that the heavy-fermion superconductivity is mediated by the quadrupole fluctuations.

In order to understand the unusual heavy-fermion superconductivity, the information of electronic structure under the normal state might be helpful. The de Haas-van Alphen (dHvA) effect is a powerful tool to investigate the electronic structure such as the Fermi surface and the effective mass. So far, we measured the dHvA effects in $PrTi_2Al_{20}$ and the reference compound $LaTi_2Al_{20}$ down to the lowest temperature of ~ 0.5 K utilizing the ^{3}He-cryostat,[12] and compared with the results of band-structure calculation in $LaTi_2Al_{20}$. However, the experimental results were insufficient because of the insufficient high-field and low-temperature conditions; the expected Fermi surface with larger effective mass was not observed in the previous experiments. In this work, we continuously study the dHvA effect down to the lowest temperature of ~ 30 mK utilizing the ^{3}He-^{4}He dilution refrigerator.

2. Experimental Details

Single crystals of $PrTi_2Al_{20}$ and $LaTi_2Al_{20}$ were grown by an Al-self-flux method which is basically the same as that of previous report.[7] We employed the molar ratio (Pr or La) : Ti : Al = 1 : 2 : 45, and used 99.9%-pure(3N)-Pr, 4N-La, 4N-Ti, and 5N-Al as raw materials. The obtained single crystals are typically ~ 1 mm^3 in size with regular octahedron shape. The single crystalline nature was confirmed by a back Laue X-ray diffraction method. The electrical resistivity measurements (not shown here) revealed that the residual resistivity ratios ($\rho_{290K}/\rho_{0.5K}$) of the present samples for $PrTi_2Al_{20}$ and $LaTi_2Al_{20}$ are about 100 and 180, respectively, indicating the high-quality of samples. The dHvA experiments were performed

both in a top loading dilution refrigerator down to ~ 30 mK with a 15 T superconducting magnet and in a conventional dilution refrigerator down to ~ 40 mK with a 17 T superconducting magnet. The dHvA-signals were detected by the conventional field modulation method with a frequency of 45 ~ 68 Hz.

3. Results and Discussion

Figures 1(a) and 1(b) show the typical dHvA oscillations in $LaTi_2Al_{20}$ and $PrTi_2Al_{20}$ for field along H // <100>, and Figs. 1(c) and 1(d) show their corresponding fast Fourier transformation (FFT) spectra. The dHvA frequency F, which is expressed as a unit of magnetic field, is proportional to the extremal cross-sectional area S_F of the Femi surface with the following relation $F = c\hbar S_F/(2\pi e)$.[13] Many dHvA-signals are observed both in $LaTi_2Al_{20}$ and

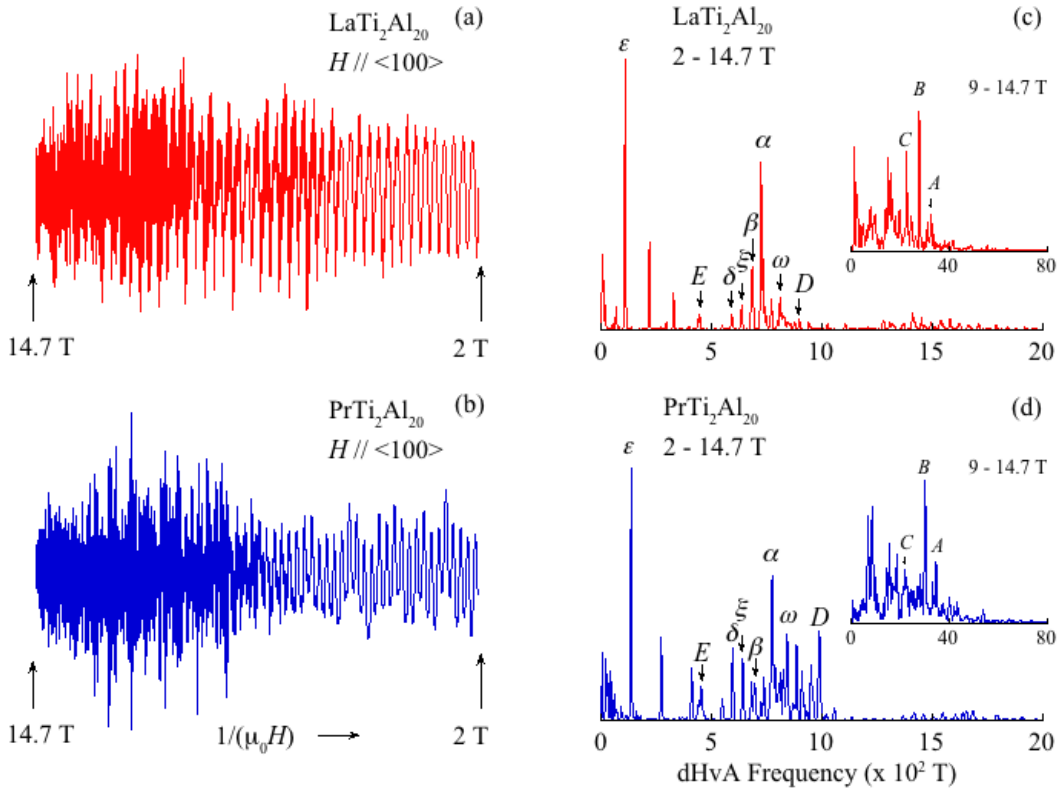

Fig. 1. (Color online) (a)[(b)] Typical dHvA oscillations for field along H // <100> and (c)[(d)] the corresponding fast Fourier transformation (FFT) spectra in $LaTi_2Al_{20}$ [$PrTi_2Al_{20}$]. The inset of (c)[(d)] shows the FFT spectra between 9 and 14.7 T.

$PrTi_2Al_{20}$ ranging from about 16 to 5400 T. In Figs. 1(c) and 1(d), the typical fundamental dHvA-signals are labeled α, β, δ, ε, ω, ξ, η, and A - E, whereas the other signals including harmonics are not labeled for the simplicity. The frequencies of signals labeled Greek letters are basically the same as those of previous report observed above ~ 0.5 K.[12] The signals labeled alphabetic letters are newly observed ones in this work.

To investigate the Fermi surface topology, we measured the angular dependence of the dHvA frequency both in $LaTi_2Al_{20}$ and $PrTi_2Al_{20}$ as shown in Figs. 2(a) and 2(b). Many other dHvA-signals mentioned above were observed, especially for the field along the H // <111> and H // <110>, suggesting the multiply-connected Fermi surface. The dHvA-frequency branches ε and δ were continuously observed in wide field-angle ranges with weak angular

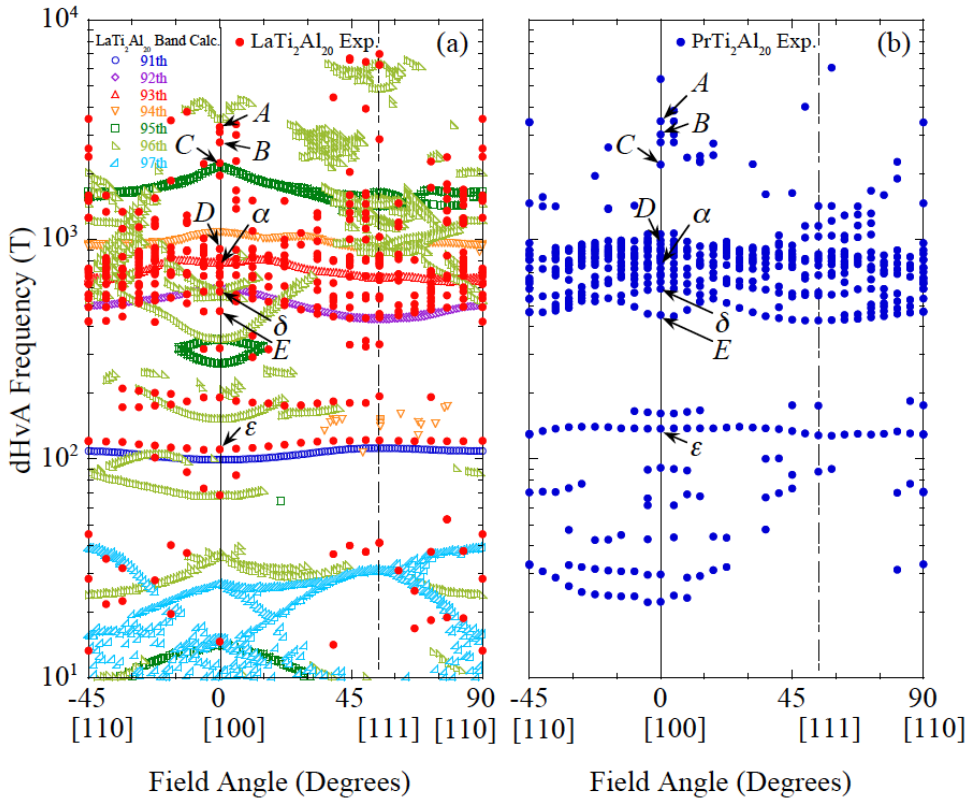

Fig. 2. (Color online) Comparison of the angular dependence of the dHvA-frequency between (a) $LaTi_2Al_{20}$ and (b) $PrTi_2Al_{20}$. The red and blue closed circles represent the experimental data for $LaTi_2Al_{20}$ and $PrTi_2Al_{20}$, respectively, and the open symbols represent the theoretical ones obtained by the band-structure calculation for $LaTi_2Al_{20}$.

dependences, indicating almost the spherical Fermi surfaces, that are also basically the same as the previous report.[12] While, the branches *A*, *B*, and *C* are observed in the limited field-angles around *H* // <100>. The origins of these frequency-branches are described later comparing with the band-structure calculation. These angular dependences are close to each other between $LaTi_2Al_{20}$ and $PrTi_2Al_{20}$, indicating almost the same Fermi surface topology between these compounds and suggesting the localized nature of 4*f*-electrons in $PrTi_2Al_{20}$.

In order to assign the origin of the dHvA-frequency branches, the band-structure calculations for $LaTi_2Al_{20}$ have been carried out based on a full-potential linearized augmented-plane-wave (FLAPW) method with in the local-density approximation (LDA); the results were partially published in the previous report.[12] The resultant band structure and its density of states are shown in Figs. 3(a) and 3(b), respectively. The bands mainly consist of Al-*p* bands and the

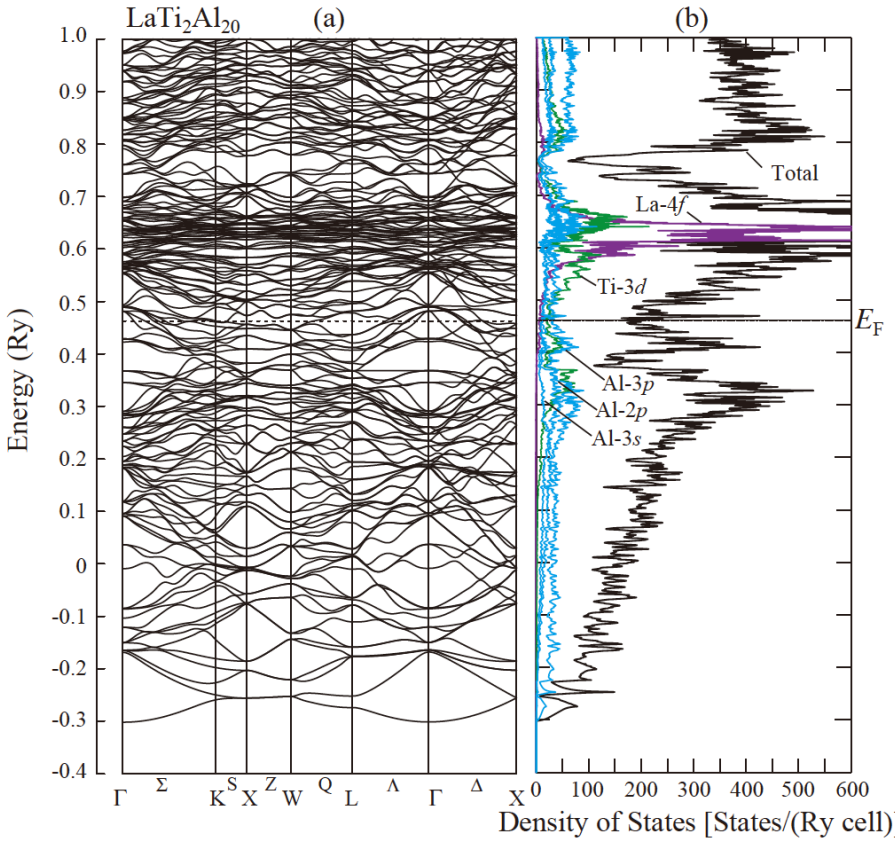

Fig. 3. (Color online) (a) Band structure and (b) its density of states of $LaTi_2Al_{20}$. Fermi energy is denoted by E_F.

Table I. Electron-components of density of states (DOS) and number of states (NOS) at the Fermi level in $LaTi_2Al_{20}$. Number of states are integrated for the valence bands.

	total	La-*s*	La-*p*	La-*d*	La-*f*	Ti-*s*	Ti-*d*	Al-*s*	Al-*p*
DOS [States/(Ry cell)]	175.089	0.247	0.170	3.276	7.161	0.459	17.563	19.267	41.015
NOS	141.998	0.274	0.311	2.216	0.654	0.667	8.252	30.449	31.247

Table II. Band-components of DOS, NOS, and carrier number *n* at the Fermi level in $LaTi_2Al_{20}$. h and e denoted in parentheses mean the type of carrier, i.e., h and e mean hole and electron, respectively. Sum of carrier number of holes is the same as that of electrons since this compound is compensated metal.

	91st-band	92nd-band	93rd-band	94th-band	95th-band	96th-band	97th-band
DOS [States/(Ry cell)]	0.642	4.560	7.514	13.506	26.820	120.338	1.7080
NOS	1.9958	1.9514	1.9127	1.8619	1.6940	0.5838	0.00034
n	0.00416 (h)	0.00858 (h)	0.08726 (h)	0.13812 (h)	0.30600 (h)	0.58380 (e)	0.00034 (e)

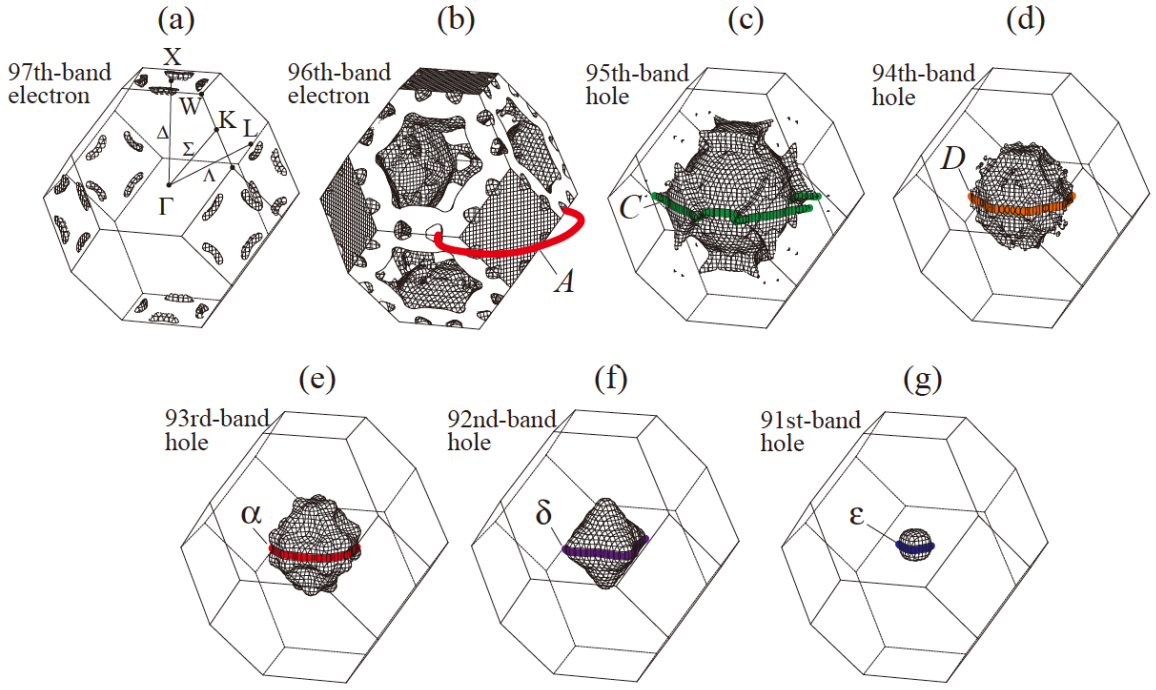

Fig. 4. (Color online) Femi surface of $LaTi_2Al_{20}$.

Fermi surface consists of seven sheets originating from the 91st-97th bands as shown in Fig. 4. The electron-components of density of states (DOS) and number of states (NOS) at the Fermi level are listed in Table I, and the band-components of DOS, NOS, and carrier number *n* of each band are listed in Table II. The total DOS at Fermi energy E_F (= 0.46201 Ry) is 175.089 states/(Ry cell), which corresponds to the Sommerfeld coefficient of 15.17 mJ/(K^2mol). As

shown in Fig. 4, the largest Fermi surface is a multiply-connected 96th-band electron sheet which is surrounding the X point and is missing for <111> directions. The 91st- 95th-band hole Fermi surfaces are closed ones which are surrounding the Γ point. The 97th-band electron Fermi surfaces are pocket ones with small carrier number. $LaTi_2Al_{20}$ is a compensated metal with equal carrier number of electrons (96th- and 97th-band sheets) and holes (91st-95th-band sheets) because the primitive cell of the crystal structure consists of two molecules.

Hereafter let us consider the origin of the dHvA-frequency branches observed in the present experiments. The theoretical angular dependence of the dHvA-frequency obtained by the band-structure calculation is shown in Fig. 2(a). Compared with the experimental data, it is evident that the branches ε and δ originate from 91st- and 92nd- bands, respectively, as already reported previously.[12] The branches α, *D, C*, and *A* might originate from the 93rd-, 94th-, 95th-, and 96th-bands, respectively, inferred from their magnitudes of the dHvA frequencies. The small branches with $F < \sim 50$ T might originate from the 96th-, and 97th-band pocket Fermi surfaces. The other dHvA-frequency branches, especially observed near δ-, α-, and *D*-branches ranging from about 600 to 1000 T, are hard to identify the origins. These unidentified dHvA-frequency branches might originate from the orbital-crossing or magnetic-breakdown of the Fermi surfaces, which are frequently observed in the compounds with non-centrosymmetric crystal structure, such as Rh_2Ga_9, Ir_2Ga_9,[14] and Yb_4Sb_3.[15] These compounds possess the small but finite splitting of Fermi surfaces due to the antisymmetric spin-orbit interaction, and the orbital crossing at the degenerate points of the split Fermi surfaces was thought to be the origin of the observed many dHvA-frequency branches. However, $LaTi_2Al_{20}$ is centrosymmetric compound so that the splitting of the Fermi surfaces is not expected, but as shown in Figs. 3(a) and 4, the 92nd-, 93rd-, and 94th-band Fermi surfaces (corresponding to δ-, α-, and *D*-branches, respectively) have degenerate or nearly degenerate points at Δ (Γ–X) and Λ (Γ–L) in the 1st Brillouin zone. Orbital-crossing or magnetic-breakdown at these degenerate points are most likely the origin of unidentified multiple dHvA-frequency branches.

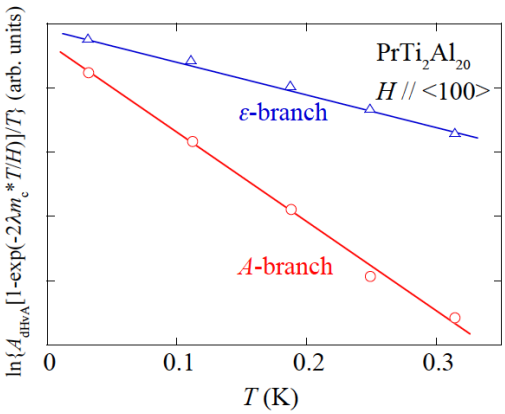

Fig. 5. (Color online) Temperature dependences of the dHvA amplitudes A_{dHvA} of ε- and A-branches for H // <100> in $PrTi_2Al_{20}$. λ in the vertical-axis label is a constant $\lambda = 2\pi^2 ck_B/(e\hbar)$. Solid lines represent the linear fitting.

As further important information, we estimated the cyclotron effective mass m_c^*. According to the Lifshitz-Kozevich formula,[13] the temperature dependence of the dHvA amplitude A_{dHvA} (magnitude of the FFT spectrum) is given by $\ln\{A_{dHvA}[1 - \exp(-2\lambda m_c^* T/H)]/T\} = -\lambda m_c^* T/H +$ const., where λ is a constant $\lambda = 2\pi^2 ck_B/(e\hbar)$. From the temperature dependence of A_{dHvA} at constant magnetic field (so-called mass plot), we estimated the m_c^* both in $LaTi_2Al_{20}$ and $PrTi_2Al_{20}$. The typical examples of mass plots for ε- and A- branches for H // <100> in $PrTi_2Al_{20}$ are shown in Fig. 5. The estimated m_c^*s compared with the results of the band-structure calculation for $LaTi_2Al_{20}$ are summarized in Table III. The experimental m_c^*s in $LaTi_2Al_{20}$ are not so large ranging from about 0.1 to 3.2 m_0, which are reasonably well explained by the band-structure calculation. While the experimental m_c^*s in $PrTi_2Al_{20}$ are evidently large ranging from about 1.3 to 12 m_0, which are about 5 times larger than those of $LaTi_2Al_{20}$. The fact is consistent with the enhancement of the Sommerfeld coefficient; the experimental Sommerfeld coefficients of $PrTi_2Al_{20}$ and $LaTi_2Al_{20}$ are $\gamma \sim 100$ mJ/(K^{2}mol) and $\gamma \sim 23$ mJ/(K^{2}mol), respectively. Thus, we directly confirmed the heavy-fermion state in $PrTi_2Al_{20}$ by the present dHvA experiments.

Here, we mention about the temperature dependence of m_c^*. The m_c^*s of $PrTi_2Al_{20}$ for H // <100>, which were determined below ~ 0.3 K in the present work, are 2.3 ~ 3.8 times larger

Table III. Comparison of the dHvA frequency F and the corresponding cyclotron mass m_c^* between $PrTi_2Al_{20}$ and $LaTi_2Al_{20}$.

		$PrTi_2Al_{20}$ (Exper.)		$LaTi_2Al_{20}$ (Exper.)		$LaTi_2Al_{20}$ (Theor.)	
Field direction	Branch	F ($\times 10^2$ T)	m_c^*/m_0	F ($\times 10^2$ T)	m_c^*/m_0	F ($\times 10^2$ T)	m_c^*/m_0
<100>	α	34.65	10.3±0.4	32.50	1.96±0.06	35.566	2.443
	β	30.04	8.5±0.1	27.70	1.10±0.02	-	-
	γ	21.84	-	22.35	0.95±0.02	21.438	1.314
	δ	9.88	2.36±0.02	9.07	0.40±0.01	10.758	0.529
	ω	8.42	1.91±0.02	8.26	0.40±0.01		
	α	7.75	2.09±0.02	7.50	0.38±0.01	7.787	0.284
	β	6.96	1.75±0.02	6.80	0.36±0.01	-	-
	ξ	6.41	1.71±0.01	6.39	0.48±0.01	-	-
	δ	5.97	1.99±0.02	5.79	0.36±0.01	5.943	0.281
	ε	4.53	3.5±0.2	4.71	1.07±0.02	3.500	0.390
	ε	1.37	1.25±0.05	1.10	0.09±0.01	0.955	0.083
<110>		34.25	12.2±0.7	35.50	3.25±0.06	20.045	1.970
		14.63	3.62±0.04	15.00	0.64±0.01	16.468	0.685
		7.44	2.83±0.04	7.38	0.36±0.01	6.691	0.307
	δ	4.66	2.59±0.01	4.91	0.35±0.01	4.952	0.224
	ε	1.30	1.98±0.03	1.21	0.11±0.01	1.077	0.094
<111>		-	-	70.15	2.44±0.01	63.222	3.894
		14.15	7.58±0.02	-	-	16.314	1.036
		10.26	3.21±0.09	10.25	1.10±0.03	9.441	0.815
		6.86	3.06±0.01	6.81	0.44±0.01	6.700	0.299
	δ	4.27	2.89±0.04	4.42	0.40±0.01	4.351	0.248
	ε	1.28	1.67±0.05	1.21	0.13±0.01	1.109	0.098

than those of our previous work above ~ 0.5 K,[12] which could not be explained by the large experimental errors about 10 ~ 20% in the previous work due to the poor mass plots performed at higher temperature ranges of 0.5 ~ 1.1 K. Such an enhancement of m_c^* with decreasing temperatures was also reported in $PrPb_3$ which exhibits an antiferro-quadrupolar order below T_{AFQ} = 0.4 K.[16] The origin of the mass enhancement was suggested to be a quadrupolar interaction because the enhancement of m_c^* became remarkable below ~ T_{AFQ}.

Finally, we compare the heavy-fermion state in $PrTi_2Al_{20}$ with other related Pr-compounds, PrV_2Al_{20} and $PrIr_2Zn_{20}$, whose CEF ground states are also the non-magnetic Γ_3 doublet. Moderately strong *c-f* hybridization effects have been suggested in $PrTi_2Al_{20}$ such as $-\ln T$ dependence of $\rho(T)$, i.e., Kondo effect, and the Kondo resonant peak of the photoemission spectroscopy. [1, 2, 11] Such a strong *c-f* hybridization thought to arise from the characteristic crystal structure of this compound; Pr atoms are encapsulated in cages formed by 16 Al-atoms so that the large coordination number results in the strong *c-f* hybridization. The hybridization strength can be enhanced not only by the physical pressure,[3] but also by the chemical one. In the sister compound PrV_2Al_{20}, an even stronger *c-f* hybridization than that of $PrTi_2Al_{20}$ has been expected because of the smaller ionic radius of V than that of Ti. Also, an additional 3*d*-electron of V in PrV_2Al_{20}, which contributes to the conduction band and enhances the density of states at Fermi energy, may enhance the *c-f* hybridization. Actually, under the ambient pressure, PrV_2Al_{20} exhibits a heavy-fermion superconductivity below T_c = 0.05 K in the antiferro-quadrupole ordered state below T_{AFQ}= 0.75 K.[4] The specific heat measurement revealed the larger Sommerfeld coefficient $\gamma \sim 900$ mJ/(K^{2}mol). Also, the larger effective mass $m^* \sim 140\ m_0$ was suggested from the temperature dependence of the superconducting upper critical field. The Shubnikov-de Haas effect (oscillation in magnetoresistance) in PrV_2Al_{20} revealed the large cyclotron effective mass $\sim 10\ m_0$ even in the small Fermi surface with F = 2000 T.[17] The stronger *c-f* hybridization in PrV_2Al_{20} than in $PrTi_2Al_{20}$, which suppresses T_{AFQ}, promotes heavier electronic state in PrV_2Al_{20}. These facts provide an interesting counterpart to the properties in the isostructural $PrIr_2Zn_{20}$ which also exhibits the superconductivity below T_c = 0.05 K in the antiferro-quadrupole ordered state below T_{AFQ} = 0.11 K.[18, 19] In contrast with PrT_2Al_{20} (T = V, Ti), the *c-f* hybridization in $PrIr_2Zn_{20}$ is thought to be rather weak from the fact that no evident Kondo effect was observed in $\rho(T)$,[18, 20] although the non-Fermi liquid behavior due to the quadrupole Kondo effect was suggested.[21] The dHvA experiments also showed the definitive evidences of well localized nature of 4*f*-electrons in $PrIr_2Zn_{20}$; the

observed dHvA frequencies were reasonably well explained by the results of the band-structure calculation for $LaIr_2Zn_{20}$ using the lattice parameters of $PrIr_2Zn_{20}$ and the small cyclotron effective masses less than 1 m_0 were observed,[20] that means the 4*f* electrons in $PrIr_2Zn_{20}$ hardly contribute to the Fermi surface. Also, the constituent Ir-5*d* and Zn-3*d* electrons in $PrIr_2Zn_{20}$ form the different electronic structure with those of PrT_2Al_{20} (T = V, Ti), which may result in the different *c-f* hybridization strength. The difference of low temperature properties of these compounds including the non-Fermi-liquid behaviors, the unusual magnetic phase diagrams, and the possible theoretical explanations for these properties were reviewed by Onimaru and Kusunose, based on the Γ_3 doublet ground state and its quadrupolar interaction.[22] The present dHvA experiments in $PrTi_2Al_{20}$ may provide the difference of *c-f* hybridization strength among these three compounds.

4. Summary

We measured the dHvA effect in $PrTi_2Al_{20}$ and its reference compound $LaTi_2Al_{20}$ down to the lowest temperature of ~ 30 mK. The feature of the angular dependence of the dHvA frequency of $PrTi_2Al_{20}$ is close to that of the reference compound $LaTi_2Al_{20}$, indicating the localized nature of 4*f*-electrons in $PrTi_2Al_{20}$, while the cyclotron masses are highly enhanced up to 12 m_0, which are about 5 times larger than that in $LaTi_2Al_{20}$. The large mass enhancement in $PrTi_2Al_{20}$ may be due to the moderate strong *c-f* hybridization which results in the unusual quadrupolar interaction such as quadrupole Kondo effect.

Acknowledgment

This work was partly supported by JSPS KAKENHI Grants Nos. JP15H05882, JP15H05884, JP15H05885, 18H04320, and 18H04321 (J-Physics).

*E-mail: sugawara@crystal.kobe-u.ac.jp

1) A. Sakai and S. Nakatsuji, J. Phys. Soc. Jpn. **80**, 063701 (2011).
2) A. Sakai, K. Kuga, and S. Nakatsuji, J. Phys. Soc. Jpn. **81**, 083702 (2012).
3) K. Matsubayashi, T. Tanaka, A. Sakai, S. Nakatsuji, Y. Kubo, and Y. Uwatoko, Phys. Rev. Lett. **109**, 187004 (2012).
4) M. Tsujimoto, Y. Mtsumoto, T. Tomita, A. Sakai, and S. Nakatsuji, Phys. Rev. Lett. **113**, 267001 (2013).
5) T. Namiki, Q. Lei, Y. Ishikawa, and K. Nishimura, J. Phys. Soc. Jpn. **85**, 073706 (2016).
6) R. Higashinaka, T. Maruyama, A. Nakama, R. Miyazaki, Y. Aoki, and H. Sato, J. Phys. Soc. Jpn. **80**, 093703 (2011).
7) A. Sakai and S. Nakatsuji, Phys. Rev. B **84**, 201106(R) (2011).
8) T. J. Sato, S. Ibuka, Y. Nambu, T. Yamazaki, T. Hong, A. Sakai, and S. Nakatsuji, Phys. Rev. B **86**, 184419 (2012).
9) M. Koseki, Y. Nakanishi, K. Deto, G. Koseki, R. Kashiwazaki, F. Shichinomiya, M. Nakamura, M. Yoshizawa, A. Sakai, and S. Nakatsuji, J. Phys. Soc. Jpn. **80**, SA049 (2011).
10) T. Taniguchi, M. Yoshida, H. Takeda, M. Takigawa, M. Tsujimoto, A. Sakai, Y. Matsumoto, and S. Nakatsuji, J. Phys. Soc. Jpn. **85**, 113703 (2016).
11) M. Matsunami, M. Taguchi, A. Chainani, R. Eguchi, M. Oura, A. Sakai, S. Nakatsuji, and S. Shin, Phys. Rev. B **84**, 193101 (2011).
12) S. Nagashima, T. Nishiwaki, A. Otani, M. Sakoda, E. Matsuoka, H. Harima, and H. Sugawara, JPS Conf. Proc. **3**, 011019 (2014).
13) D. Shoenberg: *Magnetic Oscillations in Metals* (Cambridge University Press, Cambridge, U. K., 1984).
14) M. Takeda, A. Teruya, A. Nakamura, H. Harima, M. Hedo, T. Nakama, and Y. Onuki, J. Phys. Soc. Jpn. **84**, 024701 (2015).
15) N. Kimura, H. Sano, M. Shirakawa, A. Ochiai, H. Funashima, and H. Harima, J. Phys. Soc. Jpn. **87**, 11478 (2018).

16) D. Aoki, Y. Katayama, R. Settai, Y. Inada, Y. Onuki, H. Harima, and Z. Kletowski, J. Phys. Soc. Jpn. **66**, 3988 (1997).

17) Y. Shimura, M. Tsujimoto, B. Zeng, L. Balicas, A. Sakai, and S. Nakatsuji, Phys. Rev. B **91**, 241102 (R) (2015).

18) T. Onimaru, K. T. Matsumoto, Y. F. Inoue, K. Umeo, Y. Saiga, Y. Matsushita, R. Tamura, K. Nishimoto, I. Ishii, T. Suzuki, and T. Takabatake, J. Phys. Soc. Jpn. **79**, 033704 (2010).

19) T. Onimaru, K. T. Matsumoto, Y. F. Inoue, K. Umeo, T. Sakakibara, Y. Karaki, M. Kubota, and T. Sakakibara, Phys. Rev. Lett. **106**, 177001 (2011).

20) M. Matsushita, J. Sakaguchi, Y. Taga, M. Ohya, S. Yoshiuchi, H. Ota, Y. Hirose, K. Enoki, F. Honda, K. Sugiyama, M. Hagiwara, K. Kindo, T. Tanaka, Y. Kubo, T. Takeuchi, R. Settai, and Y. Onuki, J. Phys. Soc. Jpn. **80**, 074605 (2011).

21) T. Onimaru, K. Izawa, K. T. Matsumoto, T. Yoshida, Y. Machida, T. Ikeura, K. Wakiya, K. Umeo, S. Kittaka, K. Araki, T. Sakakibara, and T. Takabatake, Phys. Rev. B **94**, 075134 (2016).

22) T. Onimaru and H. Kusunose, J. Phys. Soc. Jpn. **85**, 082002 (2016), and references therein.